第33卷 第7期　　焊　接　学　报　　Vol. 33　No. 7
2012年7月　　TRANSACTIONS OF THE CHINA WELDING INSTITUTION　　July　2012

铜基钎料焊接金刚石的界面结构与强度

关砚聪，　郑敏利，　姚德明
（哈尔滨理工大学 机械动力学院，哈尔滨　150080）

摘　要：选用Cu-Sn-Ti活性钎料在钢基体上焊接金刚石磨粒，研究钎料合金与金刚石焊接界面的组织形貌与物相组成，分析不同钎焊温度对焊接界面结构及结合强度的影响．结果表明，钎料合金元素与金刚石在钎焊过程中发生化学反应，生成化合物TiC，CuTi和CuSn等，实现了铜基钎料、金刚石颗粒与钢基体之间的化学冶金结合．当钎焊温度为880～930 ℃时，均可获得连接良好的钎焊接头；钎焊温度900 ℃时，焊接界面形成的化合物层均匀连续且界面致密，此时在相同磨削条件下，钎焊金刚石试件的磨损失重很小，达到了焊接界面的强力结合．

关键词：金刚石磨粒；焊接；铜基钎料；界面结构；结合强度
中图分类号：TG425　　**文献标识码**：A　　**文章编号**：0253－360X(2012)07－0065－04

关砚聪

0　序　　言

金刚石颗粒以其优越的性能成为加工硬脆材料不可替代的工具材料，金刚石工具广泛用于航天、航空、汽车、建筑工程和石油钻探等领域．目前工业中使用的金刚石磨具主要采用电镀制品，金刚石颗粒只被机械镶嵌在镀层中，镀层金属与基体和磨料之间没有形成牢固的化学冶金结合，在磨削加工时，磨具容易因磨粒脱落或镀层剥落导致失效．因此国外学者从20世纪90年代初以来，致力于研究钎焊金刚石技术，以期实现金刚石、钎料与基体三者之间的化学冶金结合，获得高磨削效率、长使用寿命的金刚石磨具．

从研究进展来看，目前金刚石颗粒还局限于单层金刚石工具的钎焊，整体技术尚不成熟．用于焊接金刚石的钎料主要有以Ag-Cu-Ti合金为主的银基钎料[1]和以Ni-Cr合金为主的镍基钎料[2,3]．Ag-Cu-Ti钎料熔点低，但高含银量增加焊接成本；Ni-Cr钎料熔点高，金刚石在焊接过程中容易出现热损伤，致使这些钎料的广泛应用受到一定限制．目前以Cu-Sn-Ti合金为主的铜基钎料由于性能与Ag-Cu-Ti钎料接近，成本远低于Ag-Cu-Ti钎料而备受关注．Hsieh等人[4]用Cu-Sn-Ti合金钎焊金刚石，模拟钎料对石墨润湿过程，分析了在850～1 000 ℃之间焊缝形成过程中相的演变．邓朝晖等人[5]根据超声考察了铜基钎料钎焊金刚石界面的冲击强度．

试验采用Cu-Sn-Ti铜基钎料在钢基体上焊接金刚石颗粒，研究焊接界面微观组织，分析不同钎焊温度对焊接界面结构及结合强度的影响，探讨Cu-Sn-Ti钎料对金刚石和金属基体的焊接性能．

1　试验方法

试验选用80/100MBD8型金刚石磨料，试样基体选用45钢．钎料为粉状铜基钎料，将纯度大于99.9%的铜、锌、钛的金属粉末按Cu-8Sn-11Ti（质量分数，%）配比，放入混粉瓶中混合均匀．

焊前对金刚石和钢试样进行去油污处理，钢件用800号水砂纸打磨，以利于熔融钎料在基体表面的顺利铺展和润湿．将配好的钎料和粘接剂混合后涂覆在试样表面，再将金刚石颗粒均匀排布在钎料上，如图1所示．

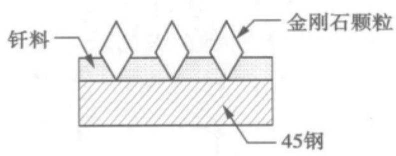

图1　钎焊金刚石颗粒示意图
Fig. 1　Schematic diagram of brazing diamond particles

焊接试验在真空炉进行，钎焊温度选择高于钎料熔点50 ℃，炉内温度先以10 ℃/min升至钎焊温

收稿日期：2012－03－26
基金项目：黑龙江省自然基金资助项目(EO124)

度，保温 10 min，随后以 5 ℃/min 降至 400 ℃，随炉冷却至室温，炉内真空度小于 0.01 Pa.

将焊好的试样进行切割，在酸中腐蚀后用丙酮清洗. 通过 FEI Sirion 扫描电镜和 EDS 能谱仪观察金刚石颗粒与钎料界面、钎料与钢基体之间的断口形貌及元素成分，通过 D/Max-rB 旋极 X 射线衍射仪对钎焊结合界面产生的化合物进行物相分析.

由于金刚石单晶颗粒的形状为不规则多面体，按标准方法很难直接测出钎料与金刚石单晶颗粒界面的结合强度. 因此通过磨削花岗石表面，测量钎焊金刚石试件的磨损失重，并在 SEM 下观察不同钎焊温度下焊接金刚石颗粒磨损后的表面形貌，以此评价金刚石钎焊界面间结合强度.

2 试验结果与讨论

2.1 钎焊接头界面组织

当钎焊温度为 900 ℃，保温时间为 10 min 时，Cu-8Sn-11Ti 钎料钎焊金刚石颗粒的形貌如图 2 所示. 从图 2 中可看出，金刚石颗粒晶形完好且边缘被钎料合金包覆，这表明 Cu-Sn-Ti 合金对金刚石颗粒表现出良好的浸润性，金刚石磨粒与钎料合金的结合界面形成了均匀、连续而致密的结合.

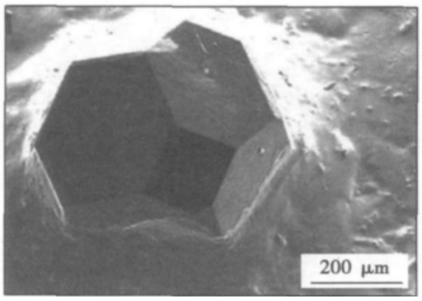

图 2 钎焊金刚石表面形貌

Fig. 2 Surface appearances of brazing diamond particles

表 1 为金刚石与钎料结合界面的定点成分分析，从表 1 可以看出，金刚石表面的 Ti 元素浓度明显高于钎料本身的浓度，表明在高温作用下 Ti 元素从钎料中向金刚石表面扩散，与金刚石发生界面反应并与金刚石中的 C 元素结合生成碳化物. 从热力学角度分析，在高温真空条件下，Ti 元素在金刚石表面的富集只有在金刚石中的碳与钎料中的钛反应后才继续扩散. 金刚石与钎料界面在反应过程中发生三种现象，一是金刚石中的碳向界面扩散，二是钛元素向界面的上坡扩散，三是碳和钛碳化物的生成.

表 1 钎焊金刚石表面定点成分分析(质量分数，%)

Table 1 Fixed-point component analysis on surface of brazing diamond

C	Cu	Sn	Ti
30.68	47.14	6.11	21.37

尽管从表 1 中已经显示出磨粒与钎料结合界面之间存在元素的扩散现象，但还不能确定界面新生化合物种类，而化合物的生成与分布形式对于磨粒与钎料层之间的结构过渡具有极其重要的影响，因为钎料层属于金属键结合材料，金刚石颗粒主要是共价键结合材料，如果能够经由化合物内部的结合键使金刚石颗粒与钎料层之间产生连接，对于提高其结合强度具有显著作用.

为判断钎焊金刚石颗粒表面新生化合物种类，对图 3 所示的 X 射线衍射进行分析，CuTi，$CuSnTi_3$ 和 CuSn 是粉状铜基钎料在钎焊过程中元素间相互作用形成的金属化合物，TiC 是新生产物，证明活性元素 Ti 与金刚石颗粒在钎焊过程中发生了化学反应. 图 3 中显示主要衍射峰分别为金刚石，Cu，TiC，CuTi 和 CuSn，其中金刚石的衍射峰最强，其次为 Cu，TiC，CuTi 和 CuSn，以及少量的 $CuSnTi_3$. 正是由于碳化物的形成，减小了金刚石与钎料的界面张力，提高了钎料的润湿性.

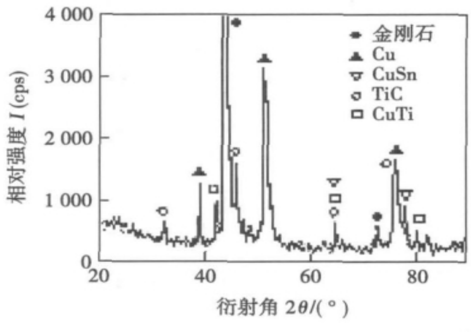

图 3 钎焊界面微区 X 射线衍射

Fig. 3 X-ray diffraction pattern of micro-domain of brazing interface

界面反应产物的形貌可反映钎料与金刚石颗粒在界面处相互作用的程度. 对钎焊金刚石进行线切割，用 800 号水砂纸打磨后进行强酸腐蚀，观察钎焊金刚石与基体的连接界面. 如图 4 所示，金刚石颗粒表面被一层反应产物所包裹，证明铜基钎料对金刚石与 45 钢基体的润湿性很好，钎料在钢基体表面完全铺展，并包裹住金刚石颗粒.

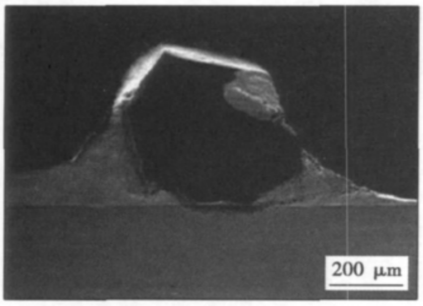

图 4　金刚石颗粒界面的微观形貌

Fig. 4　Micro features of interface of diamond particles

2.2　不同钎焊温度时钎焊界面生成物的变化

钎焊工艺参数是影响钎焊界面结合性能的重要因素. 钎焊温度影响钎料对金刚石的润湿性和元素间相互作用程度，钎焊温度、保温时间、真空度三者密切相关，综合影响界面反应产物的微观结构和结合性能.

图 5 为保温时间 10 min，不同钎焊温度时钎焊金刚石界面生成物的形貌变化. 当钎焊温度为 880 ℃时，钎料虽然熔化，但其铺展性、流动性和润湿性不充分，金刚石界面化合物晶粒尚未完全生成，不足以形成对金刚石颗粒和金属基体的较高强度连接; 当钎焊温度为 900 ℃时，钎料润湿金刚石，金刚石表面形成均匀而致密的化合物层，且具备完整的晶体形貌; 当钎焊温度为 930 ℃时，随着钎焊温度的升高，界面处的晶粒变得粗大，反应层增厚而致密性下降，如果温度过大致使界面反应激烈而增加脆性.

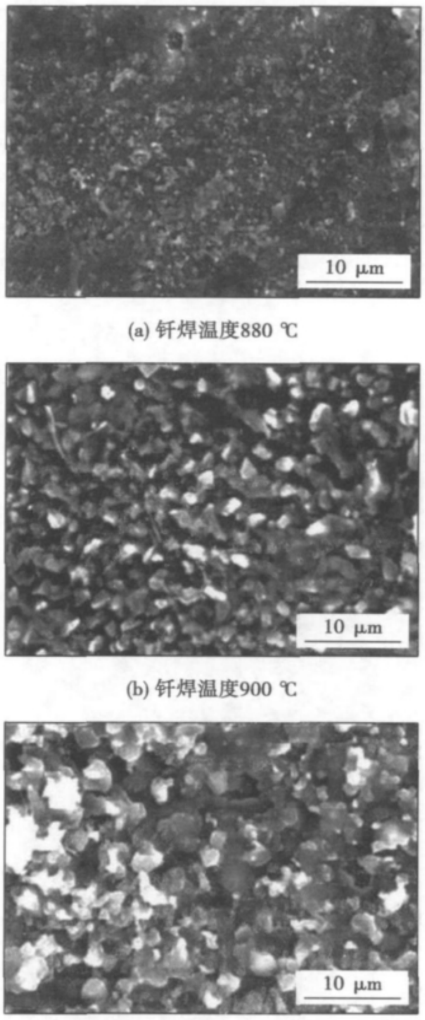

(a) 钎焊温度880 ℃

(b) 钎焊温度900 ℃

(c) 钎焊温度930 ℃

图 5　不同钎焊温度时钎焊界面化合物

Fig. 5　Compounds on brazing surface at different brazing temperatures

2.3　钎焊金刚石界面结合强度及磨损

钎焊金刚石磨具在使用过程中的磨损是一个复杂的综合过程. 磨损形式与磨削参数、金刚石颗粒的破碎及颗粒的脱落等因素密切相关. 钎焊金刚石磨具受到的摩擦力主要由金刚石颗粒承载，因此金刚石颗粒脱落是磨损的主要原因. 影响金刚石颗粒的脱落的主要因素除了磨削工艺参数外，还有金刚石与钎料间的结合强度、钎料的力学性能和钎焊界面结构，其中钎料与金刚石颗粒的结合强度起重要作用.

钎焊金刚石试件的磨损试验是在 DKT-Ⅰ 型多功能石材加工机床上进行的，试验旋转速度为 2 960 r/min，加冷却水，被磨削试件选用 80 mm × 30 mm × 20 mm 的巴西黑花岗石. 金刚石磨损失重的测量采用丹佛 TP214 型电子天平(量程 260 g，精度 0.1 mg) .

表 2 为在不同钎焊温度条件下钎焊金刚石试件的磨损失重. 由表 2 可以看出，当钎焊温度为 880 ℃时，试件出现失重，这是由于钎焊温度较低，钎料中的活性元素与金刚石相互作用的结合强度不够大所致; 当钎焊温度为 900 ℃时，试件失重较少，这是由于钎焊温度升高，活性元素与金刚石相互作用充分，形成化合物型界面，结合强度提高; 钎焊温度为 930 ℃时，试件失重增大，这是由于温度高时，活性元素与金刚石相互作用加剧，界面反应产物增加且晶粒变得粗大，致使结合强度降低.

表 2　不同钎焊温度下金刚石试件磨损重量

Table 2　Diamond specimens weightlessness at different brazing temperatures

钎焊温度 T/℃	磨损重量 ΔW/mg
880	2.3
900	0.9
930	1.4

图 6 为当钎焊温度为 900 ℃，保温时间为 10 min 时，Cu-8Sn-11Ti 钎料钎焊金刚石颗粒磨损后的表面形貌. 金刚石颗粒在磨削过程中主要有不同程度的块状破碎(图 6a) 和磨平(图 6b) 等状态，图 6c 所示为金刚石试样磨损的情况，由图 6c 可以看出金刚石颗粒和基体尽管磨损严重，但很少看到金刚石颗粒整体脱落的情况. 当金刚石破损或被磨平失去切削能力时，金刚石颗粒仍很好的包埋在钎料层中，这表明用铜基钎料钎焊金刚石颗粒可实现强力的化学冶金结合，金刚石颗粒的利用率和金刚石磨具的使用寿命得到了提高.

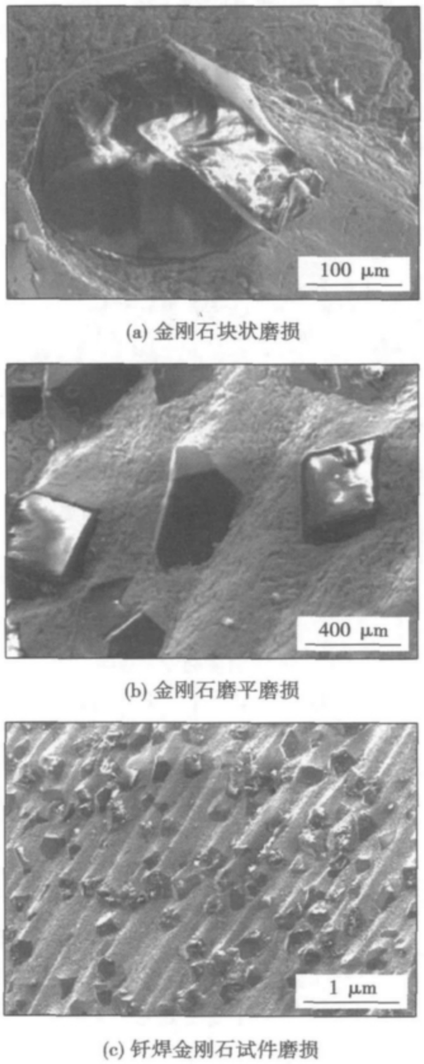

(a) 金刚石块状磨损

(b) 金刚石磨平磨损

(c) 钎焊金刚石试件磨损

图 6 钎焊金刚石试件磨损后的表面形貌

Fig. 6 Wearing surface appearances of test-pieces of brazing diamond

3 结 论

(1) 利用 Cu-10Sn-5Ti 钎料对金刚石颗粒进行了真空钎焊，钎料合金元素与金刚石在钎焊过程中发生化学反应，生成化合物 TiC，CuTi 和 CuSn 等化合物，其中 TiC 是实现金刚石与钎料之间化学结合的主要原因.

(2) 钎焊温度为 880 ~ 930 ℃，保温时间为 10 min，可实现对金刚石的冶金结合.

(3) 钎焊温度为 900 ℃时，钎料充分润湿金刚石，金刚石表面形成均匀而致密的化合物层，且具备完整的晶体形貌，此时金刚石磨损失重最小为 0.9 mg，界面结合强度最高.

参考文献:

[1] 卢金斌，徐九华. Ag-Cu-Ti 钎料钎焊金刚石的界面微观组织分析[J]. 焊接学报，2007，28(8) : 29 - 32.
Lu Jinbin，Xu Jiuhua. Analysis of interface microstructure of Ag-Cu-Ti solder braze welding diamond[J]. Transactions of the China Welding Institution，2007，28(8) : 29 - 32.

[2] 肖 冰，徐鸿钧，武志斌. Ni-Cr 合金真空单层钎焊金刚石砂轮[J]. 焊接学报，2001，22(2) : 23 - 26.
Xiao Bing，Xu Hongjun，Wu Zhibin. Ni-Cr alloy vacuum single layer braze welding diamond grinding wheel[J]. Transactions of the China Welding Institution，2001，22(2) : 23 - 26.

[3] 陈 燕，徐鸿钧，傅玉灿，等. Ni-Cr 合金真空钎焊金刚石的表面石墨化[J]. 焊接学报，2009，30(9) : 21 - 24.
Chen Yan，Xu Hongjun，Fu Yucan，*et al*. Surface graphitization of Ni-Cr alloy vacuum braze welding diamond[J]. Transactions of the China Welding Institution，2009，30(9) : 21 - 24.

[4] Hsieh Y C，Lin S T. Microstructural development of Cu-Sn-Ti alloys on graphite[J]. J Alloys and Compd，2008，466(1/2) : 126 - 132.

[5] 邓朝晖，伍俏平，张荣辉，等. 铜基钎料真空钎焊镀钛金刚石[J]. 硅酸盐学报，2011，39(2) : 343 - 348.
Deng Zhaohui，Wu Qiaoping，Zhang Ronghui，*et al*. Cu-base filler meter vacuum brazing Ti-coated diamond[J]. Journal of the Chinese Ceramic Society，2011，39(2) : 343 - 348.

作者简介: 关砚聪，女，1961 年出生，博士研究生，教授，硕士生导师. 主要从事硬脆材料加工和金刚石磨具研制方向的科研和教学工作. 发表论文 20 余篇. Email: ghx61@163.com

Optimum simulation and soldered joints reliability of WLCSP device ZHANG Liang[1,2], HAN Jiguang[1], GUO Yonghuan[1], HE Chengwen[1] (1. School of Mechanical and Electrical Engineering, Jiangsu Normal University, Xuzhou 221116, China; 2. Provincial Key Laboratory of Advanced Welding Technology, Jiangsu University of Science and Technology, Zhenjiang 212003, China). pp 53 – 56

Abstract: A quarter of WLCSP device was selected for finite element modelling and the stress-strain response of lead-free soldered joints was investigated systematically. The stress of soldered joints is variational with different positions in WLCSP array, the lowest stress of soldered joints appears in the center of array, the largest stress can be found in the outmost solder joints. The relationship between stress and position of soldered joints is as follows: $\sigma(x,y) = 1.78x + 1.78y + 0.33$, for creep strain, the correlation is: $\varepsilon(x,y) = 0.006x + 0.006y + 0.009$. Moreover, it is found that the reliability of soldered joints can be influenced by the materials in WLCSP structure, the lower reliability of soldered joints can be found in WLCSP device with polymers than that without it, so it is suitable to select the materials with matched CTE to be utilized in those devices. The reliability of WLCSP device soldered joints decreases when the pin count increases. The higher pin count means larger distance from the outmost soldered joint to the chip center at constant pitch.

Key words: WLCSP144; soldered joints array; coefficient of thermal expansion; chip center

Measurement of Q390 steel welding CCT curve ZHAO Yongtao[1], DONG Junhui[2], MA Yonglin[1], ZHOU Junwei[3] (1. Material and Metallurgy Engineering School, UST Inner Mongolia, Baotou 014010, China; 2. Materials Science and Engineering, Inner Mongolia University of Science and Technology, Huhhot 010051, China; 3. Steel-making Factory, Iron and Steel Group Company, Baotou 014010, China). pp 57 – 60

Abstract: By simulating Q390 steel welding condition, by means of thermal-dilatometer, continuous cooling transformation curve of Q390 steel was measured by Gleeble1500 thermal-simulator, at the same time, the microstructure of different cooling velocity was observed and analyzed by OM and SEM. SH-CCT curve was obtained through continuous cool character analysis and contrast. The results show that phase transformation region contains three parts: the ferrite and pearlite transition zone at high temperature, the bainite transition zone at moderate temperature and the martensite transition zone at low temperature. The microstructure including ferrite, pearlite and granular bainite can be obtained when the cooling velocity is between 0.015 and 0.1 ℃/s; lots of bainite structure can be obtained at 0.5 – 1 ℃/s cooling rate range; the martensite and residual austenite microstructure be obtained when the cooling velocity is beyond 25 ℃/s.

Key words: Q390 steel; thermal-simulation; SH-CCT

An open architecture control system of special arc-welding robot for intersection welding seam REN Fushen[1], CHEN Shujun[2], GAO sheng[1], CHANG Yulian[1], LIU Caiyu[1] (1. School of Mechanical Science and Engineering, Northeast Petroleum University, Daqing 163318, China; 2. School of Mechanical Engineering and Applied Electronics Technology, Beijing University of Technology, Beijing 100022, China). pp 61 – 64

Abstract: Based on the PC + PMAC control mode, an open architecture control system of special arc-welding robot was developed for welding seam of intersection. The trinity logic control model of welding trajectory control, welding torch pose control and welding parameters control were put forward based on welding seam, which realized the real meaning of integrated control for welding robot movement and the welding power parameters. Two control methods of PPC and CDC were put forward and a hierarchical architecture of control system software was established, which realized the state detection of the welding process. The experimental results show that the control system has strong adaptability, good portability and can accomplish the welding of seam of intersection well.

Key words: arc welding robot; welding seam of intersection; trinity; continuous data control; planning parameters control

Interfacial structure and strength of Cu-based filler metal welding diamond GUAN Yancong, ZHENG Minli, YAO Deming (Power Machinery Institute, Harbin University of Science and Technology, Harbin 150040, China). pp 65 – 68

Abstract: Cu-Sn-Ti active filler metal was selected to weld the diamond particles on the steel matrix. The organization features and phase compositions of the weld interface of solder alloy and diamond and were studied and the influences of brazing temperature on the interfacial structure and the bond strength were analyzed. The results show that solder alloy elements and diamond had chemical reaction in the process of brazing and compounds such as TiC, CuTi, and CuSn, were generated and the chemical metallurgical combination among Cu-based filler metal, diamond particles and the steel matrix were obtained. When the brazing temperature reaches to 880-930 ℃, soldered joints with good connection can be obtained. When the brazing temperature reaches to 900 ℃, the compound layer emerging on the weld interface is homogeneous, continuous, fine and close. At this moment, under the same grinding conditions, the abrasion weight loss of the brazed diamond specimen is very small, and the powerful bond of the weld interface is achieved.

Key words: abrasive particle of diamond; weld; Cu-based filler metal; interfacial structure; bond strength

Effect of Pr on whisker growth of Sn-Zn-Ga lead-free solder CHEN Cheng[1], XUE Songbai[1], YANG Jingqiu[2], YE Huan[1], LI Yang[1] (1. College of Materials Science and Technology, Nanjing University of Aeronautics and Astronautics, Nanjing 210016, China; 2. Harbin Welding Institute, Harbin 150000, China). pp 69 – 72

Abstract: Relation between Sn whisker growth and the amount of rare earth was studied. The influence factor of Sn whisker growth was initially analyzed, especially in the aspect of aging time and cooling rate. Furthermore, the growth mechanism of Sn whisker growth on the surface of the solder was initially discussed. The experimental results show that with the addition of 0.7% Pr to Sn-Zn-Ga-xPr solder, Sn whisker could spontaneously grow on the surface of the solder only after aging 12 hours. With the increasing of aging time, the length of Sn whisker grew rapidly, which could reach the critical value of failure after aging